https://doi.org/10.5194/egusphere-2026-2099
Preprint. Discussion started: 23 April 2026

Tree-microbe-soil interactions affecting soil organic carbon fractions in Mediterranean forest soils

Stav Livne-Luzon[a†], Assaf Yaakobi[a†], David Yalin[b], Dagan Sade[c], Efrat Dener[d,e], Yaara Oppenheimer-Shaanan[a,f], Tamir Klein[a]

[a] Plant & Environmental Sciences Department, Weizmann Institute of Science, Rehovot 7610001, Israel

[b] The Israel Agricultural Research Organization (Volcani Institute), Rishon LeZion 7505101, Israel

[c] Biomolecular Sciences Department, Weizmann Institute of Science, Rehovot 7610001, Israel

[d] Albert Katz International School for Desert Studies, Jacob Blaustein Institutes for Desert Research, Ben Gurion University of the Negev, Sede Boqer Campus, Midreshet Ben-Gurion, Israel

[e] Mitrani Department of Desert Ecology, Swiss Institute for Dryland Environmental and Energy Research, The Jacob Blaustein Institutes for Desert Research, Ben-Gurion University of the Negev, Sede Boqer Campus, Midreshet Ben-Gurion, Israel

[f] Department of Life Sciences, Achva Academic College, Arugot, 79804, Israel.

[†]Co-Lead authors: Stav Livne-Luzon and Assaf Yaakobi

Corresponding author: Stav Livne Luzon stavl@weizmann.ac.il, +972-8-934-3505

Keywords: Soil organic carbon (SOC); Mineral-associated organic carbon (MAOC); Particulate organic carbon (POC); Mediterranean forests; Soil texture; Microbial communities.

https://doi.org/10.5194/egusphere-2026-2099
Preprint. Discussion started: 23 April 2026

Abstract

Soil organic carbon (SOC) represents a major terrestrial carbon pool, yet the processes that regulate its storage remain uncertain, particularly in water-limited ecosystems. The behavior of SOC is informed by partitioning into mineral-associated organic carbon (MAOC), considered more persistent, and particulate organic carbon (POC), which is more labile. We investigated how SOC fractions were affected by forest tree species, including *Pinus halepensis* (a canopy conifer), *Quercus calliprinos* (a sub-canopy broadleaf), and *Pistacia lentiscus* (an understory woody shrub) as compared to mixing of these species, focusing on shallow-soil mature Mediterranean stands. To elucidate further insights, the effects of soil physicochemical properties and microbial community were examined. Across soil samples, SOC concentrations were up to twofold higher under tree canopies compared to forest gaps with *Quercus* plots storing 10–30% more SOC than *Pinus* and *Pistacia* plots. SOC variation was primarily explained by POC, for which mixed plots showed increased concentrations as compared to monospecific plots. In contrast, MAOC displayed a saturation pattern (maximum ~ 45 g C kg^{-1} soil), strongly constrained by clay and silt content, with apparent high saturation levels. Mixed forests supported seasonally stable microbial communities but did not consistently increase microbial diversity. Bacterial composition was shaped by microsite conditions, with soils under tree canopies harboring subsets of the more diverse forest-gap communities. Overall, despite the fact that mixed forest increased microbial richness, this effect did not propagate to affect the different soil C pools. Nevertheless, the effect of forest type on soil C pools was modulated by specific microsites and tree-species characteristics. For instance, transitioning to mixed forests could increase SOC by approximately 6.1 Mg C ha^{-1} compared to monospecific pine forests, but this carbon is expected to primarily be stored in the labile POC pool, especially in soils near saturation.

https://doi.org/10.5194/egusphere-2026-2099
Preprint. Discussion started: 23 April 2026

1. Introduction

Soil organic carbon (SOC) comprises one of the largest terrestrial carbon pools, containing more carbon than terrestrial vegetation and the atmosphere combined (Lal et al. 2021). The distribution of SOC varies widely across latitudes, with the highest concentrations in northern regions, followed by tropical, temperate, and Mediterranean forests being the poorest (Crowther et al. 2019).

Ongoing and predicted climate changes, induced by rising atmospheric CO_2 concentrations and land use changes, are expected to significantly impact terrestrial ecosystems and specifically the SOC pools (Gregorich et al. 2017, Nissan et al. 2023). However, the fate of SOC is still poorly constrained in land-models, in large part due to lack of empirical data from specific ecosystems and especially drylands (Arora et al. 2013, Stell et al. 2021). To this end, there is great importance in better understanding the drivers behind SOC dynamics in these ecosystems. Additionally, because afforestation and improved forest management are proposed as some of the leading natural climate mitigation options, there is need to understand how these can be best adapted for enhanced SOC capturing (Griscom et al. 2017).

SOC dynamics are governed by a complex interplay between plant carbon inputs, microbial activity, soil fauna, and the soil matrix (Cotrufo and Lavallee 2022). The critical role of soil properties in determining SOC accumulation in soil has been demonstrated in several global studies. Doetterl et al.(2015), for example found that soil properties such as clay + silt were the main predictors for SOC storage (exceeding the role of climate) along a 4000 km climate transect of natural grassland and shrubland in Chile and the Antarctic Peninsula. Later work examining data from continental USA has shown that other soil factors than clay + silt such as exchangeable calcium strongly predicted soil organic matter (SOM) content in water-limited, alkaline soils for example (Rasmussen et al. 2018).

To decipher the mechanisms behind SOC storage, the distinction between the mineral-associated organic carbon (MAOC) and particulate organic carbon (POC) can be highly informative (Cotrufo et al. 2019). The interactions of MAOC with the soil mineral phase protects it from microbial decomposition, resulting in prolonged cycling time of up to millennia (Schmidt et al. 2011). MAOC is mostly comprised of small organic molecules with a low C/N ratio (e.g. polysaccharides, proteins, lipids) originating in microbial necromass and root exudates (Whalen et al. 2022). In contrast, POC is mainly comprised of more complex organic molecules (e.g. lignin, cellulose, hemicellulose) with a high C/N ratio, and goes

https://doi.org/10.5194/egusphere-2026-2099
Preprint. Discussion started: 23 April 2026

through faster cycling (typically decades) due to high exposure to decomposition. Globally, MAOC comprises approximately 65% (~ 840–1540 Pg C) of the total SOC (Sokol et al. 2022) and this dominance of the MAOC pool was also reported specifically in drylands (Díaz-Martínez et al. 2024).

Because of their different nature, the accumulation of POC is governed by different ecosystem properties as compared to MAOC. For instance, a meta-analysis by Hansen et al. (2024) found that the POC fraction across ecosystems was dominated by temperature and pH, seemingly due to the strong effect of these parameters on microbial degradation. Contrastingly, MAOC has shown strong correlation to the fine mineral fraction (clay + silt) content.

It has been argued that MAOC has a finite capacity that is the upper limit for its accumulation in soils, which may in part explain the close relation between MAOC and soil texture. The specific soil capacitance according to this perception is related to its clay + silt content and the mineralogy of these fractions (Georgiou et al. 2025). Based on data from soils in the USA it was estimated that soil with high reactivity minerals have a capacitance of 86 g C kg^{-1} clay + silt, whereas soils with low activity clays have a capacitance of 48 g C kg^{-1} clay + silt (Georgiou et al. 2022). These capacitance values also correspond with findings from other studies showing a saturation of MAOC in a wide array of soils at values close to 40 g C kg^{-1} soil (Cotrufo et al. 2019). However, it is unclear if MAOC capacitance can be a true limiting factor for MAOC accumulation and especially in low productivity ecosystems.

Forest composition affects SOC storage in many levels – tree species deliver varying amounts of organic matter to soil through leaf litter, root exudates, and also support distinct microbial communities (Lindahl and Tunlid 2015, Obersteiner and Klein 2022). The effects of forests and afforestation on SOC is therefore context dependent. In a study of over 600 control and afforested plot pairs in China, afforestation was found to increase SOC only in SOC-depleted soils, while high-SOC soils responded to afforestation with SOC losses (Hong et al. 2020). In that study, tree species had a significant effect on SOC accumulation or loss. Similar context-dependent SOC accumulation was also shown in other meta-analysis studying the effects of afforestation (Ll et al. 2012). Dıaz-Pines et al. (2011) demonstrated variations in SOC content across three different forest types, with pine forests showing the highest levels of MAOC and POC, while oak forests showing the lowest. Mixed forests fall in between, indicating a moderate carbon accumulation. In another meta-analysis

https://doi.org/10.5194/egusphere-2026-2099
Preprint. Discussion started: 23 April 2026

encompassing a wide variety of ecosystems, plant diversity was shown to have a general positive effect on SOC storage, especially in dry regions (Spohn et al. 2023).

Rog et al. (2022), has previously shown that the composition of forest ecosystems can play a critical role in shaping belowground dynamics. Avital et al., (2022) observed asymmetric C transfer between different tree species cohabitating Mediterranean mixed forests. These patterns could potentially lead to increased SOM accumulation in mixed forest settings as compared to monoculture forests. However, it should also be considered that trees typically form complex, mutualistic symbioses with both fungi and bacteria, influencing their community composition and the SOC and nitrogen dynamics (Lucas-Borja et al. 2012).

Overall, despite significant advances in understanding SOM dynamics, including the development of next-generation biogeochemical models and large-scale datasets, the interactions between tree species composition, soil properties and microbial communities, and their effects on SOC pools remain inadequately understood (Cotrufo and Lavallee 2022). The limited and sometimes contradictory empirical evidence points to the need for more rigorous, species-specific research to elucidate these relationships. Clarifying how forest composition influences SOC storage and turnover is crucial for developing informed forest management practices that maximize carbon sequestration in response to climate change (Amelung et al. 2020).

This study aims to evaluate the influence of tree and forest composition (tree species and mixing) on SOC pools. We sampled soil in mixed and monospecific plots of various compositions in a Mediterranean forest, focusing on tree species representing the key functional groups in this ecosystem. Specifically, we included *Pinus halepensis* (a canopy conifer), *Quercus calliprinos* (a sub-canopy broadleaf), and *Pistacia lentiscus* (an understory woody shrub). The studied plots were managed by the local forest service (Jewish National Fund (KKL)) with native tree species and minimal intervention. The key research questions are: (1) How does forest type (tree species and mixing) influence total SOC stocks and the distribution between MAOC and POC? And how does this relate to soil microbial diversity? (2) Is soil limited in its capacity to store MAOC?

We hypothesize that mixed forests will exhibit higher total SOC stocks, with a greater proportion of MAOC compared to mono-specific forests, due to enhanced microbial diversity and more efficient organic matter stabilization. Additionally, we expect that soil properties, particularly capacitance (clay + silt content), will modulate the partitioning of SOC, with

https://doi.org/10.5194/egusphere-2026-2099
Preprint. Discussion started: 23 April 2026

higher soil capacitance favoring MAOC storage. We further hypothesize that forest gaps, due to reduced organic input and microbial activity, will exhibit lower total SOC and a higher POC fraction. To test these hypotheses, we used sequential equation modeling (SEM) to explore the direct and indirect effects of forest mixing, microsite, tree traits, and soil properties on SOC dynamics (Fig.1a), providing insights into the complex interactions that drive carbon storage in Mediterranean forests.

2. Materials and Methods

2.1. Study site and experimental design

Field measurements were conducted in Yishi Forest in the Judean foothills, Israel (Fig. 1b; Rog et al. (2021a)). The climate in this area is characterized as hot Mediterranean, with a mean annual precipitation of 510 mm between September and May and mean daily temperatures of 16.0°C in February and 25.3°C in August. The predominant soil types in the study area are Ustolls (Mollisols;(Itkin et al. 2025)), forming a thin soil layer (5-20 cm) over a limestone bedrock. The vegetation is dominated by the gymnosperm tree species *Pinus halepensis*, which forms the forest canopy, partly with the lesser canopy gymnosperm tree species, *Cupressus sempervirens.* The sub-canopy layer is dominated by the angiosperm tree species *Quercus calliprinos*, and the understory is dominated by the angiosperm woody shrub *Pistacia lentiscus*. Additionally, a variety of annual plants flourish from winter to spring in gaps between trees at the forest floor. These smaller plants have biomass of ~8.22×10^{-5} kg C m^{-2}, compared with 61.8 kg C m^{-2} of e.g., the *Pinus* trees, and hence a disproportionally smaller contribution to the forest C cycle (for additional information on the tree species, see Table S1). Root and litter C content and flux were calculated for each of the three species. Root system in the soil layer was calculated as described in Rog et al. (2021b) by integrating (1) sampling of forest soil cores around each of the study trees and measurement of lateral root biomass in each core; (2) identification of excavated roots (5-20 cm depth) around each of the study trees, based on DNA barcodes (Jakoby et al. 2020); (3) upscaling the measurements in (1) and (2) to the entire soil layer based on stand density information and allometric relationships for each of the species, based on stem diameter and height and applying asymptotic equations for the distribution of root biomass in depth (Jackson et al. 1996). Root system in the rock layer was estimated based on the difference between the soil root biomass calculated in (3) and the total root biomass, calculated by species-specific

https://doi.org/10.5194/egusphere-2026-2099
Preprint. Discussion started: 23 April 2026

allometric equations. Annual root growth was measured using the ingrowth core method (Rog et al. 2024). Annual root litter was estimated using our root biomass calculations (above) and the global patterns of root turnover in terrestrial ecosystem database (Gill and Jackson 2000). Annual aboveground litter was quantified using litter traps installed below the canopy of each tree species and collected bi-monthly (Rog et al. 2024). Annual root exudation was calculated in Rog et al. (2024), based on *in situ* and *ex situ* root exudation measurements (Jakoby et al. 2020 and , Dror and Klein 2022, respectively). For simplicity, we will refer to the species by their genus names: *Pinus*, *Quercus* and *Pistacia*. We chose representative plots for the mixed forest with a combination of all three species mentioned above, and three monospecific plots, each composed of only one of the three tree species. The term 'mixed' refers to plots containing multiple tree species, rather than, for example, soil samples pooled from different plots (not done here). As for the monospecific plots, for *Pinus*, *Quercus*, and *Pistacia*, we found plots that were dominated by these species rather than pure monospecific (Fig. 1a-c; Table S2). The *Pinus* plot was planted in 1968; the *Quercus* and the *Pistacia* plots were naturally germinated; and the mixed plots were planted the same year as the *Pinus* but developed into a mixed forest. To account for the effect of tree diversity, we chose five individual representative trees in each plot. Next to each tree, we collected two samples at 0-1 m from the trunk in opposite directions. In addition, we sampled three soil samples from a forest gap (2-3 m from the canopy; Fig. 1b) in each plot. All soil samples were collected at a depth of 0-10 cm, representing the thin soil layer at the site (n = 104 soil samples).

2.2. Soil sampling and plot characteristics

In September 2022, soil sampling was conducted across all designated plots. Multiple sample types were obtained at each sampling point, including plant litter, undisturbed sampling for bulk-density measurements, and disturbed samples for SOC, other chemical analyses, and microbial community composition analysis. Plant litter was collected at each designated sampling point within the study area using a frame measuring 0.3 m × 0.3 m. The collected litter was then placed in individual paper bags. Subsequently, the plant litter was dried at 60°C for several days until it reached a constant weight. Soil cores were extracted using a stainless-steel soil core sampler kit with a core radius of 4.8 cm. The soil within each core was air-dried for at least seven days. After the drying period and sieving to 2 mm, the mass of each soil sample was determined by weighing, and bulk density was subsequently calculated.

https://doi.org/10.5194/egusphere-2026-2099
Preprint. Discussion started: 23 April 2026

Soil samples for carbon and chemical analysis were collected at the site of litter collection and in close proximity (<1 m) to the undisturbed sampling pits. In the spring of 2023, measurements of annual plant richness were taken from each plot at the same locations used for forest-gap sampling. Plants were collected within a 0.3 m × 0.3 m frame, and the number of species and individuals within each species were recorded (Table S2).

2.3. Soil fractionation methods and carbon analysis

The soil samples were air-dried in the lab for at least seven days at ambient room temperature with proper ventilation. Wet separation of soil fractions larger than 50 µm (sand) and smaller than 50 µm (clay + silt) was performed following Poeplau et al. (2018) using 0.5% Na-hexametaphosphate and agitation with glass beads for the degradation of soil aggregates. In tandem soil texture analysis was performed using PARIO (Meter, Munich, Germany) following the manufacturer's protocol (Fig. S1). SOC, total nitrogen and soil inorganic carbon in the separate fractions and bulk soil samples were determined using an elemental analyzer (EA; Elementar, Cheadle, UK, Model: soli TOC cube). SOC values reported include the total organic carbon combusted up to 600 °C. Measurements with the elemental analyzer were conducted on both bulk soil and the fine fraction (particles < 50 µm). For the coarse fraction, organic carbon content was derived by subtracting the fine fraction from the bulk soil. Comparing the results for MAOC and SOC from the elemental analyzer to those obtained by traditional loss on ignition (Fig. S2) revealed a strong linear relationship, particularly for MAOC. Consequently, further analyses and data presented in this paper focus on the results from the elemental analyzer.

2.4. Soil structure, moisture, and nutrient content

Soil water content (%, v/v) and soil temperature (°C) were measured over depths of 0-15 cm (i.e., the entire soil profile in our shallow soil site) using a portable soil sensor (Acclima, Meridian, ID, USA; SDI-12 Sensor Reader RD1200). Measurements were taken at two time points: summer and spring. All records were collected during the day, and measurements from all plots were taken on the same day to avoid temporal effects. Three data points were recorded from each plot at each position (forest gap and under trees), except in the mixed plots, where data were recorded from under all five trees. All records were obtained from the same locations where the soil samples were collected. Soil nutrient analysis (excluding phosphorus), electrical conductivity (EC), and pH were performed using water extracts of 8 g

https://doi.org/10.5194/egusphere-2026-2099
Preprint. Discussion started: 23 April 2026

air-dried soil with 32 ml of deionized distilled water shaken overnight. pH measurements were conducted using a pH meter (VWR phenomenal, PH 1100 L, UK; n = 104). EC was measured using an EC Meter (Model 4510, Jenway, England; n = 104). Major anions, including chloride (Cl^-) and nitrate (NO_3^-), as well as major cations, including ammonium (NH_4^+) and magnesium (Mg^{2+}), were analyzed using the Gallery Analyzer (Thermo Scientific, Germering, Germany). Available phosphorus (P) was extracted following Olsen (1954) and analyzed using the Gallery Analyzer.

2.5. Analysis of microbial community composition

To survey soil microbial communities, we employed a hybrid approach for large-scale, high-resolution microbial profiling of novel environmental niches (Fuks et al. 2018, Knafo et al. 2023). The analysis is described below, step by step.

Sample Collection, Preservation, and DNA Extraction

Soil subsamples were collected from the previously described "bulk soil" using sterile 2 mL tubes, kept on ice during transport to the laboratory. Upon arrival, samples were immediately stored at −80°C and later transferred into specialized perforated tubes for three-day lyophilization. Lyophilized samples were then stored at −20°C until DNA extraction.

Soil samples were collected in two sampling campaigns: once in summer 2022 and again in spring 2023. The collection protocol was consistent across both seasons and locations: surface litter was removed, the upper 0-10 cm of soil was excavated, homogenized, and placed into sterile 2 mL tubes. DNA was extracted from approximately 250 mg of soil using an automated extraction workflow on a Tecan liquid-handling robot, employing the ZymoBIOMICS™ 96 MagBead DNA Kit (Zymo Research, Irvine, CA, USA; Cat. No. D4308) according to the manufacturer's protocol.

Short Reads Library Preparation and Sequencing

Short-read amplicon libraries were prepared using a two-step PCR strategy. The first PCR was designed to linearly amplify targeted regions of the 16S rRNA gene (six variable regions: V1V2, V2V3, V3V4, V4V5, V5V7, and V7V9) as well as the fungal ITS1 and ITS2 regions. This amplification incorporated an Illumina-compatible read sequence, a stepper sequence to introduce sequence diversity, and a Unique Molecular Identifier (UMI) for error correction and duplicate removal (Rezenman et al. 2023). The second PCR was performed to add Illumina i5/i7 indexes and further amplify the amplicons. All libraries were then pooled and

https://doi.org/10.5194/egusphere-2026-2099
Preprint. Discussion started: 23 April 2026

concentrated using KAPA beads (0.65X) and sequenced on the Illumina NovaSeq platform using a 151|10|10|151 cycle configuration, yielding between 12.5K and 1.5M reads per sample.

Amplicon Processing and Data Analysis

Each sample was demultiplexed by variable region using Cutadapt (Martin, 2011), as described in the CoSMIC pipeline (Knafo et al. 2023), excluding any long, non-specific amplicons generated during PCR. Paired-end reads (R1 and R2) were then quality-filtered and denoised using the DADA2 package in R (Callahan et al. 2016), which corrects for sequencing errors and generates high-resolution amplicon sequence variants (ASVs). The resulting bacterial sequences were subsequently submitted for taxonomic profiling using the Short multi-Region Framework (SMURF) algorithm (Fuks et al. 2018). Libraries for 16S rRNA gene were prepared following a custom 16S region protocol developed in Reich lab (Weizmann Institute of Science). This amplification aimed at capturing a broad representation of the microbial community by targeting multiple variable regions in the 16S gene. The resulting amplicons were indexed to create a next-generation sequencing (NGS) library, with each index corresponding to a unique sample. Sequencing was carried out on an Illumina NovaSeq platform (2 × 150-bp paired ends), generating short, high-quality reads. Reads were analyzed using the SMURF algorithm to generate the most likely microbial composition and ratios of a given sample (Fuks et al. 2018). To attain a detailed description of a given population, SMURF algorithm requires the full-length small subunit (SSU) to appear in the given data set. Given that environmental samples are often underrepresented in common databases, a long-read sequencing application using PacBio was developed to retrieve full-length SSU sequences from pooled samples. This approach allows for a more accurate resolution of microbiome composition (Knafo et al. 2023). 16S rRNA full-length amplicons, obtained from the LNA amplification of microbial communities in soil samples, were used as a starting template for the SMRTbell Express template Prep Kit 2.0 kit (Product PN. 100-938-900). The sequencing was done on the PacBio Sequel Sequencer. An initial analysis step of demultiplexing, filtering, and removal of chimeric reads was performed using the SMRT analysis software. We used the SILVA database standard threshold for their NR99 database and clustered our samples with 99% identity. Short reads sequencing was subsequently analyzed by the augmented-database SMURF. All Scripts and usage instructions appear in the GitHub repository rezenman/CoSMIC. The amplicon sequence

https://doi.org/10.5194/egusphere-2026-2099
Preprint. Discussion started: 23 April 2026

variants (ASVs) were derived from the provided dataset, with taxonomic data including Kingdom, Phylum, Class, Order, Family, Genus, and Species. Bacterial richness, diversity, and composition were processed and analyzed using the phyloseq R package. The resulting sequences and their respective frequencies were then used to assess the richness and diversity of the samples and compare the microbial communities among and between forest types and microsites.

2.6. Statistical analysis

To assess differences in all response variables (including SOC, its fractions MAOC and POC, carbon stocks, carbon saturation, bacterial richness, and diversity), a mixed-effects model was fitted using the 'lmer' function from the 'lme4' R package. Fixed effects for 'forest type' (Mixed forest vs. Monospecific forest), 'microsite' (Forest gap, under *Pistacia*, under *Pinus* or under *Quercus* canopies), and their interaction were included in the model, along with a random effect for 'tree' to account for repeated measures of individual trees within plots. The significance of the fixed effects was assessed through an analysis of variance (ANOVA) conducted using the 'Anova' function from the 'car' package, which allowed for the evaluation of the main effects and interactions within the model. Post-hoc pairwise comparisons were performed using Tukey's Honest Significant Difference (HSD) test to explore differences among levels of the 'forest type' and 'microsite' factors. Estimated marginal means for the interaction between 'forest type' and 'microsite' were obtained using the 'emmeans' package. Specific comparisons (i.e., contrasting forest gaps with all other tree canopy samples) were adjusted for multiple comparisons using the False Discovery Rate (FDR) method.

In addition, to identify potential drivers of SOC and its fractions, we analyzed the relationships between twelve measured soil properties (e.g., bulk density, pH, soil temperature, nutrient levels) and SOC, MAOC, and POC. Each soil property was tested in individual mixed-effects models with the same structure (forest type and microsite as fixed effects; tree as a random effect). Continuous variables were scaled to improve comparability. Multicollinearity among predictors was visualized using a correlation plot (Fig. S3). We then performed Principal Component Analysis (PCA) on standardized soil physicochemical variables to summarize multivariate patterns among samples. Ellipses representing 95% confidence intervals were added to visualize group separation by forest type.

https://doi.org/10.5194/egusphere-2026-2099
Preprint. Discussion started: 23 April 2026

Finally, microbial diversity analyses were conducted in R (version 4.2.2). Taxonomic data and abundance matrices were processed using the phyloseq (version 1.42.0; (McMurdie and Holmes 2013) and microViz (version 0.11.0) packages (Barnett et al. 2021). Beta diversity was assessed using Principal Coordinates Analysis (PCoA) based on Bray–Curtis dissimilarities, calculated with the microViz package (version 0.11.0). Ordination plots were generated using functions from both microViz and phyloseq. Permutational multivariate analysis of variance (PERMANOVA) and tests of multivariate dispersion (beta-dispersion) were conducted to assess the effects of forest type, microsite, and season on community structure. To examine taxonomic composition, phylum-level relative abundances were calculated, and the top 10 most abundant phyla were visualized in a proportional stacked bar plot across microsites. Differentially abundant bacterial genera between under canopies and forest gaps were identified using ANCOM-BC (Lin and Peddada 2020). Results were visualized using a bar plot of log-fold changes, highlighting top taxa showing significant differences based on false discovery rate (FDR)-adjusted P values. Relationships between ecological diversity indices (bacterial species richness and Shannon diversity in spring and summer) and SOC, MAOC, and POC were assessed using linear regressions with Pearson correlation coefficients, and were visualized using faceted scatterplots.

2.7 Path modeling

To examine the complex relationships between ecological variables across hierarchical levels in our dataset, we utilized structural equation modeling (SEM), allowing us to simultaneously assess multiple direct, indirect, and overall total effects of the tested variables on soil carbon fractions (Fig. 1a). The model was built *a priori* to reflect the hierarchical structure of our data, testing biologically plausible paths among variables. Specifically, we tested the effects of forest type (mono vs. mixed), microsite (e.g., *Pinus*, *Pistacia*, *Quercus*, and forest gap), tree species traits (aboveground biomass and litter density), soil properties (using the PC1 axis from the soil physicochemical PCA, see above) as well as the soil clay + silt content, and microbial community richness on the soil carbon fractions (MAOC, POC).

The relationships between forest type, microsite, and ecological variables were specified through direct effects, with additional paths including biomass, litter density, and other soil properties influencing carbon pool variables. Additional effects across hierarchical levels, such as the effect of microsite on soil properties, were modeled as well, but only appear in the final model if their contribution to the total effects was significant. Forest type was treated as

https://doi.org/10.5194/egusphere-2026-2099
Preprint. Discussion started: 23 April 2026

a dummy-coded exogenous variable (0 = Mono, 1 = Mixed), and microsite was modeled as an ordered factor, with the order determined by canopy cover (1->2->3->4). All continuous dependent variables were centered.

The initial model fit was assessed using several indices, including the Comparative Fit Index (CFI), Tucker-Lewis Index (TLI), and Root Mean Square Error of Approximation (RMSEA). To achieve a better model fit, we then ran a refined version of the model in which we removed the non-significant correlations. Bootstrapped standard errors and p-values were used to evaluate the significance of the paths. All analyses were conducted using R (version 4.0.0) with the lavaan and semTools packages (Jorgensen et al. 2012, Rosseel 2012).

3. Results

3.1. Forest composition effect on soil organic carbon and litter pools

Soil organic carbon (SOC) concentrations in our shallow soil site ranged between 18.3 and 187.1 g C kg^{-1} soil across tree species and microsites, with the highest values recorded under *Quercus* and the lowest in a forest gap in a mixed plot (Fig. 2; Table S3). SOC significantly varied among forest microsites (microsite: $\chi_3 = 18.8$, $p < 0.001$). Notably, SOC under tree canopies was up to 2-fold higher than in forest gaps (Fig. 2; Table S3), with the effect being most pronounced under *Quercus* in monospecific plots (contrast forest gap vs. under *Quercus* canopy: $t_{16.8} = -3.04$, $p = 0.021$). Monospecific plots had an overall lower SOC than mixed forest plots but this pattern was only marginally non-significant (Fig. 2, $\chi_1 = 3.30$, $p = 0.069$), and this was mainly attributed to elevated SOC under *Pistacia* canopies in the mixed plot as compared to the mono specific plot (contrast mixed vs. mono-forests: $t_{25.5}=2.60$, $p = 0.015$). Considering in situ soil depths, densities, and stone fractions, we calculated SOC stocks for each plot. SOC stocks to a depth of 10 cm (most of the entire, 15 cm deep profile) ranged from 1 kg C m^{-2} in monospecific forest gaps and *Pistacia* plots, to 2 and almost 3 kg C m^{-2} in *Pinus* and mixed *Quercus* plots, respectively (Fig. S4). The MAOC fraction did not significantly differ among forest types nor between microsites (Fig. 2). Therefore, the trends in SOC mainly reflected those in the POC fraction. Yet, the trends in POC were more marginal so that the difference in mixed-forest plots under canopies of *Pistacia* and *Quercus* were minor compared to forest gaps (contrast forest gap vs. under *Quercus* canopy: $t_{18.4} = -2.84$, $p = 0.062$; contrast forest gap vs. under *Pistacia* canopy: $t_{19.0} = -2.29$, $p = 0.096$). In the monospecific plots, there was only a significant difference between the POC under the tree

https://doi.org/10.5194/egusphere-2026-2099
Preprint. Discussion started: 23 April 2026

canopies and forest gaps for *Quercus* (contrast forest gap vs. under *Quercus* canopy: $t_{18.1}$ =-2.91, p = 0.027).

Litter dry mass significantly differed among microsites (χ_3 = 38.91, p < 0.001), with higher values observed under *Pistacia*, *Pinus*, and *Quercus* canopies compared to forest gaps (Fig. S5a). There was no significant difference among forest types (χ_1 = 0.15, p = 0.69) however there was a significant interaction between forest type and microsite (χ_3 = 8.23, p = 0.041). Overall, *Quercus* tended to accumulate more litter compared to all other tree species, especially in mixed plots (contrast mixed vs. mono-forests: $t_{24.3}$ = -2.07, p = 0.049).

The C/N ratios of the bulk soil organic matter (SOM), and of the fine fraction organic matter (i.e., mineral-associated organic matter, MAOM) showed variable responses to forest type and microsite (Fig. S5b). For SOM, there was a significant difference among microsites (χ_3 = 8.89, p = 0.030) and a marginally non-significant effect of forest type (χ_1 = 3.31, p = 0.068), indicating context-dependent differences across microsites and forest compositions.

3.2. Mineral associated organic carbon saturation behavior

Overall, the Clay + silt content in our forest soil averaged around 63%, ranging from 28% to 92%. MAOC exhibited a saturation-type relationship with increasing SOC across sites (Fig. 3a), reaching a maximum of 35.5 g C kg^{-1} soil. At lower SOC levels, MAOC comprised nearly 80% of the SOC pool, but its saturation behavior led to a declining relative contribution, so that POC accounted for more than 90% of total SOC at high-SOC sites. Across plots, MAOC increased linearly with clay + silt content (χ_1 = 21.29, p <0.001; Fig. 3b). The soil MAOC capacitance for the research area was established using previously described methodology (Six et al. 2024), to yield a value of 50.3 g C kg^{-1} clay + silt (according to the top 95th percentile of the data). The C saturation, i.e., the measured MAOC as a percentage of the maximum predicted MAOC per plot was then calculated. C saturation according to this methodology ranged 40-212% and varied among microsites (χ_3 = 12.07, p = 0.007). Additionally, a significant difference was observed between the C saturation under the tree canopies and forest gaps for *Quercus* (contrast forest gap vs. under *Quercus* canopy: $t_{19.4}$ =-2.68, p = 0.043; Fig. 3c).

3.3. Underlying soil properties influencing soil organic carbon fractions

https://doi.org/10.5194/egusphere-2026-2099
Preprint. Discussion started: 23 April 2026

Twelve soil parameters were tested for their individual effects on POC and MAOC using a set of individual mixed regression models (Fig. 4a). For MAOC, there was a significant increase in MAOC with increasing clay + silt content. The soil bulk-density, soil pH and soluble magnesium were also significant predictors of the MAOC content. For POC, the bulk soil C/N ratio was the strongest predictor of C content. Other parameters like litter dry mass, soil EC, water-soluble magnesium, water-soluble inorganic nitrogen, and carbonates content ($CaCO_3$ equivalent), showed a positive relation to POC, while others demonstrated a negative relationship (clay + silt content, bulk-density, soil temperature, soil pH and extractable phosphate).

Principal component analysis (PCA) revealed a clear separation of forest plots along PC1 and PC2, which together explained 51.2% of the total variance (Fig. 4b, c). Along with PC1, positive scores were associated with higher bulk-density, pH, and extractable phosphate, whereas negative scores reflected higher litter dry mass, inorganic nitrogen, EC, and magnesium. PC2 primarily contrasted higher carbonates content and C/N ratio (positive loadings) with higher temperature, phosphate, and chloride (negative loadings). PERMANOVA tests showed that forest plots significantly differed among forest types ($F_{1,32}$=4.09, p = 0.002, R^2=0.11) and microsites ($F_{3,32}$=2.05, p = 0.021, R^2 =0.17), with mono-specific *Quercus* plots showing a significant contrast to forest gaps (PERMANOVA pairwise contrast: $F_{3,12}$ =8.18, p_{adjust} = 0.030, R^2 =0.44).

3.4. Soil microbial communities in different forest compositions

The sequencing of the 16S rRNA gene yielded a total of 1,531 ASVs, belonging to 20 phyla, 48 classes, 101 orders, 153 families, 265 genera and 2003 species. Our database enrichment using PacBio analysis revealed 413 novel full-length SSU sequences, representing unidentified bacterial species that were not present in the existing database. Considering the contrasting *in situ* wet/dry season conditions, samples were taken in spring and summer, respectively. Overall, soil microbial richness was higher in spring (107.4±17.5) than summer (65.2±13.8; season: χ_1 = 6.74, p <0.001; Fig. 5a). Generally, mixed forest plots tended to have higher microbial richness vs. the monospecific plots (74.9 ± 18.9 vs. 44.7 ± 14.7 and 155 ± 37.4 vs. 76.3 ± 13.1 for summer and spring, respectively; Fig. 5a). However, this difference was not significant, likely due to the large variations among seasons and tree species. The highest soil microbial richness was in forest gaps in mixed forest plots, reaching

https://doi.org/10.5194/egusphere-2026-2099
Preprint. Discussion started: 23 April 2026

>200 species. Microbial Shannon diversity demonstrated similar patterns to those of microbial richness. No clear or consistent patterns were observed between any of the diversity indices and SOC or its fractions (MAOC and POC; Fig. S6). There was a significant compositional difference among microsites (i.e., under *Pistacia*, *Pinus*, *Quercus* trees or forest gaps) (PERMANOVA: microsite; Pseudo $F_{3,76}$=1.65, p = 0.004; Fig. 5b). This effect did not appear to result from differences in dispersion ($F_{3,76}$=0.85, p = 0.47) but rather from differences in group centroids. Overall, bacterial communities collected under trees (*Pistacia*, *Pinus*, or *Quercus*) were subsets of the bacterial communities found in forest gaps (Fig. 5c). By contrast, there were no significant differences between forest types (mixed vs. monospecific forest) (PERMANOVA: Forest type; Pseudo $F_{1,78}$=0.98, p = 0.423; Fig. 5c) nor sampling seasons (spring vs. summer) (PERMANOVA: Season; Pseudo $F_{1,78}$=1.08, p = 0.298). However, there was a significant three-way interaction among forest type, microsite, and sampling season (PERMANOVA: Interaction; $F_{15,64}$=1.16, p = 0.023). Consistent with this, bacterial composition based on Bray–Curtis distances showed a weak, marginally non-significant correlation with POC (p = 0.094) and an even weaker association with MAOC (p = 0.16). The top ten most common bacterial phyla partitioned well among the microsites, with *Pinus* soils hosting a higher proportion of proteobacteria and *Quercus* soils hosting a relatively higher proportion of *firmicutes* (Fig. 5d). ANCOM-BC analysis found no significant differences between *Pistacia* samples collected under canopies and those in forest gaps. In *Quercus*, under-canopy soils showed higher differential abundance of *Bradyrhizobium*, *Nocardioides*, and a genus within Nitrosomonadaceae. *Pinus* exhibited the largest log2-fold changes, with higher under-canopy abundance of *Pseudolabrys*, *Bradyrhizobium*, and *Tardiphaga* relative to forest gaps (Fig. 5e).

3.5 The direct and indirect effects of forest characteristics on POC and MAOC

We used structural equation modeling (SEM) to assess the direct, indirect, and total effects of ecological variables on soil carbon fractions, considering the hierarchical structure of our dataset. The model tested the influence of forest type, microsite, tree species traits, soil properties, and microbial community richness on soil carbon fractions (MAOC and POC; the conceptual model is described in Fig.1 and the final model total effects are shown in Fig. 6).

3.5.1 Model fit

https://doi.org/10.5194/egusphere-2026-2099
Preprint. Discussion started: 23 April 2026

The final structural equation model showed acceptable fit to the data (χ^2 = 20.25, df = 17, p = 0.262). Incremental fit indices were high (CFI = 0.983, TLI = 0.980), and residual-based indices indicated acceptable model performance (RMSEA = 0.056; SRMR = 0.061). Scaled fit indices showed similar trends (scaled CFI = 0.926; scaled TLI = 0.909; scaled RMSEA = 0.095). The final model explained 43.0% of the variance in MAOC and 66.3% of the variance in POC. Explained variance was 65.4% for PC1, 58.0% for litter density, 37.8% for biomass, and 14.1% for microbial community richness.

3.5.2 Direct effects

As expected, Microsite had a significant positive effect on aboveground biomass (β = 0.615, p < 0.001) and on litter density (β = 0.761, p < 0.001). PC1 of soil properties was significantly positively related to litter density (β = 0.654, p < 0.001) and negatively to clay + silt content (β = -0.411, p < 0.001). Microbial community richness showed a significant direct relationship with forest type (β = 0.376, p = 0.002). Still, it did not have a significant effect on MAOC or POC fractions, so these relations were excluded from the final model.

For soil carbon fractions, MAOC was significantly affected by soil properties (β = 0.624, p < 0.001) and clay + silt content (β = 0.761, p < 0.001). POC showed significant direct effects from soil properties (β = 0.639, p = 0.001) and microsite (β = 0.659, p = 0.005), whereas direct effects of litter density (β = -0.411, p = 0.094) and clay + silt content (β = -0.205, p = 0.082) were not statistically significant.

3.5.3 Indirect effects

Significant indirect effects on MAOC were detected for litter density through soil properties (β = 0.437, p = 0.003), for clay + silt content through soil properties (β = -0.223, p = 0.006), and microsite via the sequential pathway microsite → litter density → soil properties (β = 0.274, p = 0.002). For POC, a significant positive indirect effect was detected for litter density via soil properties (β = 0.419, p = 0.037) and a negative effect for clay + silt content through soil properties (β = -0.262, p = 0.007).

3.5.4 Total effects

Estimating the total effects (direct + indirect) indicated that forest type had a significant positive effect on microbial community richness, but was unrelated to any of the other factors. Microsite had a positive effect on both the MAOC (β = 0.274, p = 0.002) and POC

https://doi.org/10.5194/egusphere-2026-2099
Preprint. Discussion started: 23 April 2026

fractions (β = 0.466, p <0.001). Clay + silt content had a positive total effect on MAOC (β = 0.427, p <0.001) but a negative effect on POC (β = -0.509, p <0.001). Litter density only had a significant effect on MAOC (β = 0.357, p = 0.003) but not on POC. Soil properties (PC1) had a significant total effect on MAOC (β = 0.544, p < 0.001) and POC (β = 0.639, p = 0.001).

4. Discussion

This study provides a comprehensive analysis of organic carbon storage in forest soils, exploring the roles of tree species and their mixing, through physical, chemical, and biological perspectives on SOC and its fractions. Overall, we calculate that integration of mixed forest species in these Mediterranean conditions can add ~0.61 kg C m^{-2} which are ~6.1 Mg C ha^{-1}. Our holistic approach allowed us to identify key factors influencing soil carbon storage in Mediterranean shallow-soil forests (Fig. 6).

4.1. Contrasting controls on mineral-associated and particulate organic carbon

Our findings underscore how different controls dominate the accumulation of POC as compared to MAOC. POC was affected by forest composition, with mixed plots accumulating higher POC and demonstrating a subsequent higher SOC content than monospecific plots, confirming our first hypothesis. The significant control of soil factors such as pH, carbonates content and Mg on the POC and the relatively high POC values measured here may point at unique POC preservation mechanisms occurring in calcareous dryland soils as suggested by Rasmussen et al. (2018). However, studies relating to unique preservation mechanisms of SOC in calcareous soils are scarce (Rowley et al. 2018). Our findings suggest that higher nitrogen, whether organic, inorganic, or mixed, can increase POC more than MAOC, as reported in other studies (Averill and Waring 2018, Wu et al. 2023). The significant effect of C/N ratio found in our analysis might also point at N deficiency as a driver retarding POC degradation, because nitrogen availability plays a crucial role in regulating carbon cycling and storage in terrestrial ecosystems (Vitousek and Howarth 1991, Ye et al. 2018). In addition, litter with lower C/N ratios is more readily transformed into MAOC through microbial activity or direct absorption to mineral surfaces (Lavallee et al. 2018). Notwithstanding, it may also be the result of an artifact created by the weighted

https://doi.org/10.5194/egusphere-2026-2099
Preprint. Discussion started: 23 April 2026

increase in high C/N POC. Overall, our mixed forest plots demonstrated a higher C/N ratio than the mono-specific plots (42.26±5.3 for mixed vs. 31.27±2.5 in mono-specific forests), which might explain the higher POC preservation in the mixed forest.

Counter to POC, MAOC showed saturation behavior, peaking at ~45 g C Kg^{-1} soil in this study. This is in good correspondence with the work of Cotrufo et al., (2019) who showed similar saturation of MAOC at around 40 g C kg^{-1} for an extensive set of soils from across Europe. This saturation pattern and the strong dependence of MAOC on clay + silt content, both support the notion that MAOC accumulation can be constrained by the finite capacity of soil minerals for association (Georgiou et al. 2025). As MAOC is considered the more recalcitrant and larger SOC fraction, these findings further reinforce the view that soil texture is a dominant control on long-term organic carbon accumulation in soil (Doetterl et al. 2015, Rasmussen et al. 2018).

4.2. Saturation of the MAOC fraction

Using the top 95th percentile as an estimate of the soil MAOC capacitance, we established a value of 50.3 g C kg^{-1} soil for the research area. This value is close to 48 g C kg-1 established by Georgiou et al., (2022) for "low activity" mineral soils. This matches the high content of carbonate minerals in our site, typically less reactive compared to Fe and Al oxides.

Georgiou et al., (2025) noted that systems may reach an apparent saturation at values below the mineral capacity to carry MAOC due to ecosystem constraints such as water limitation. To assess this hypothesis, we examined the MAOC capacitance in a large set of dryland forests using the recently published data of Díaz-Martínez et al. (2024). That dataset yields a higher MAOC capacitance of 70.2 g C kg^{-1} clay + silt supporting the idea that in our site, mineral properties, rather than climate, were the limiting factor on MAOC accumulation.

MAOC saturation values, expressed as the percentage of the MAOC capacitance currently filled in each sampling point, exceeded 50% even in the forest gaps. Representing values above the global average for forest soils (Georgiou et al. 2022). Under such saturated conditions, it is not surprising that differences between forest gaps and under-canopy soils do not emerge as previously reported in other dryland forests (Díaz-Martínez et al. 2024). Notwithstanding, while plots with oaks (mixed and monospecific) and *Pistacia* in mixed plots were at 80-90% of MAOC saturation, plots with pines were around 70%, and other

https://doi.org/10.5194/egusphere-2026-2099
Preprint. Discussion started: 23 April 2026

plots (forest gaps and monospecific *Pistacia*) were at 60% (Fig. 3c) perhaps demonstrating the importance of organic matter quality on its accumulation (Castellano et al., 2015; Córdova et al., 2018).

4.3. Soil microbial richness and diversity across different forest types

In contrast to our hypothesis, microbial diversity was not higher in mixed vs. mono-specific plots. However, we observed higher species richness and diversity in forest gaps compared to samples taken under tree canopies, particularly in mixed forests and during spring. This pattern may be attributed to reduced competitive exclusion and niche specialization under more variable conditions. Conversely, the more stable microenvironment under tree canopies likely favors a few dominant genera, leading to reduced bacterial richness (Fig. 5a). Importantly, our analysis reflects the soil's total profile of microbial species, not only decomposers, indicating a broader ecological role of microbial communities beyond organic matter breakdown. Interestingly, neither bacterial richness nor diversity correlated with any of the SOC pools, regardless of the season (Fig. S6). However, community composition appears to be weakly correlated with POC, yet this pattern was non-significant (Fig. 5c; p =0.094). This underscores the importance of overall microbial composition and specific microbial groups in C cycling. Previous studies have shown that tree roots actively recruit specific soil bacteria, as demonstrated in *Cupressus sempervirens* (Oppenheimer-Shaanan et al. 2022). Further, increased root exudation rates during the dry season have been observed, such as in *C. sempervirens* and *Pistacia lentiscus* (studied here) which may promote bacterial growth (Jakoby et al. 2020, Oppenheimer-Shaanan et al. 2022). This aligns with Yuste et al., (2014), who found more pronounced drought responses in summer, but contrasts with Yuste et al., (2011), who did not find a correlation between bacterial biomass and SOC. Our study revealed that soil bacterial community composition was significantly shaped by microsite conditions, whereas forest type and season alone had no overall significant effects. Specifically, the tree species-specific abundant bacterial taxa (Fig. 5e) are known to play key roles in nitrogen fixation (*Bradyrhizobium* (Peoples et al. 2021) and *Microvirga* (Wolińska et al. 2017)), nitrification (Nitrosomonadaceae (Hayatsu et al. 2021)), and degradation of aromatic compounds (Nocardioides (Ma et al. 2023)), highlighting the ability of each tree species to select microbial partners that meet its nutritional and ecological needs. Conversely, under tree canopies, we observed a decrease in general soil bacteria and fewer rhizosphere-

https://doi.org/10.5194/egusphere-2026-2099
Preprint. Discussion started: 23 April 2026

associated taxa, such as *Microlunatus*, involved in phosphate cycling, and *Microvirga* and *Gaiella*, known for diverse soil functions (Fierer and Jackson 2006, Ardley et al. 2012). Notably, we observed significant interactive effects on community composition among forest type, microsite, and season, suggesting context-dependent community dynamics. Pairwise comparisons further clarified these patterns: in monospecific forests, bacterial communities exhibited significant seasonal shifts ($p = 0.008$), indicating lower compositional stability. In contrast, mixed forests maintained similar bacterial community composition across spring and summer ($p = 0.294$), reflecting higher seasonal stability. This greater stability in mixed forests may result from diverse tree species providing more continuous or heterogeneous resource inputs and buffering microenvironmental fluctuations, as suggested in this forest system (Rog et al. 2021b) and others (e.g., Urbanová et al. 2015, Baldrian 2017).

4.4 Integrating the direct and indirect effects on MAOC and POC fractions

The structural equation model partially supported our hypotheses regarding the controls on SOC partitioning (Fig. 6). Consistent with expectations, soil properties (PC1) exerted strong total effects on both MAOC and POC, and clay + silt content was positively associated with MAOC while showing a negative total effect on POC, supporting the hypothesis that higher soil capacitance favors mineral-associated carbon storage. Litter density contributed to MAOC indirectly through soil properties, in line with the expectation that organic inputs promote MAOC formation via soil-mediated pathways but showed no total effect on POC. Contrary to our hypothesis that the microbial community would play an indirect role in SOC fractionation, microbial richness, despite being significantly affected by forest type, did not explain variation in either carbon fraction (MAOC, POC) and was therefore excluded from downstream pathways. Similar non-significant qualitative results were obtained when including other metrics of the microbial community in the path analysis (i.e., microbial diversity/composition indexes). Microsite (i.e., tree species or under-tree vs. forest gap) effects on SOC were largely indirect and mediated by litter density and soil properties; however, the presence of a direct microsite effect on POC indicates that vegetation type-associated differences influence POC beyond aboveground litter inputs. This pattern is consistent with an additional contribution of belowground inputs that differ among vegetation types, including interspecific variation in root exudation and root turnover. Although belowground traits were not quantified at a resolution that enabled inclusion in the SEM, measurements from adjacent plots indicate substantial differences in root exudation rates

https://doi.org/10.5194/egusphere-2026-2099
Preprint. Discussion started: 23 April 2026

among the studied tree species (Obersteiner 2026). Overall, these results suggest that SOC fractionation in this system is primarily governed by soil physical properties and vegetation-mediated inputs, with limited support for a direct role of microbial diversity in regulating MAOC and POC stocks at the scale examined.

4.4. Study limitations and Conclusion

In discussing the limitations of this study, several key factors must be considered. First, our sampling was restricted to the top 10 cm of soil, which, while capturing the most biologically active layer, may not fully represent deeper soil processes or variations in organic matter distribution that could affect overall findings. Another limitation is that some monospecific plots were not entirely pure (Table S2), potentially introducing variability from the presence of non-target species, which could confound the results and complicate the interpretation of tree species' influence on soil properties. Furthermore, absence of data on litter quality, such as nitrogen content and micronutrient levels, further limits our understanding of how different tree species affect decomposition and soil organic matter dynamics. Nevertheless, these limitations do not undermine the validity of our study. Variability from non-target species does not overshadow the clear trends associated with tree species. While the lack of litter quality data is a constraint, the observed relationships between tree species and soil organic matter dynamics remain strong. Overall, we show that forest type can affect soil C pools through specific microsites and tree-species characteristics. Moreover, our study establishes a solid foundation for future research, contributing to a deeper understanding of the complex interactions between tree species, soil organic matter, and microbial communities.

Acknowledgments: The authors would like to thank the Jewish National Fund (KKL) for providing access to the study plots. AY thanks Yuval Steinberg and The Weizmann Tree Lab members for assistance in field sampling and lab measurements. We also wish to thank Jose Grunzweig for his friendly review of earlier drafts of this MS.

Funding: The study was supported by the Israel Council for Higher Education (VATAT project "Negative Emissions Testing Center: Standardized Evaluation of Existing and Emerging CO_2 Removal Technologies").

https://doi.org/10.5194/egusphere-2026-2099
Preprint. Discussion started: 23 April 2026

Author contributions: AY led the study under the supervision of TK, SLL, and YOS. SLL and AY performed the data analysis. DY instructed the soil analysis; DS instructed the microbial analysis; YOS instructed the chemical analysis; AY, SLL, DY and TK wrote the manuscript with help from all authors.

Data availability statement: All data used in this study is reported in the paper and the Supplementary material. Sequence data will be made available on request; upon acceptance, we will deposit data to the National Center for Biotechnology Information Sequence Read Archive and update with the accession code.

References

Amelung, W., D. Bossio, W. de Vries, I. Kögel-Knabner, J. Lehmann, R. Amundson, R. Bol, C. Collins, R. Lal, and J. Leifeld. 2020. Towards a global-scale soil climate mitigation strategy. Nature communications **11**:5427.

Ardley, J. K., M. A. Parker, S. E. De Meyer, R. D. Trengove, G. W. O'Hara, W. G. Reeve, R. J. Yates, M. J. Dilworth, A. Willems, and J. G. Howieson. 2012. Microvirga lupini sp. nov., Microvirga lotononidis sp. nov. and Microvirga zambiensis sp. nov. are alphaproteobacterial root-nodule bacteria that specifically nodulate and fix nitrogen with geographically and taxonomically separate legume hosts. International journal of systematic and evolutionary microbiology **62**:2579–2588.

Arora, V. K., G. J. Boer, P. Friedlingstein, M. Eby, C. D. Jones, J. R. Christian, G. Bonan, L. Bopp, V. Brovkin, and P. Cadule. 2013. Carbon–concentration and carbon–climate feedbacks in CMIP5 Earth system models. Journal of Climate **26**:5289–5314.

Averill, C., and B. Waring. 2018. Nitrogen limitation of decomposition and decay: how can it occur? Global Change Biology **24**:1417–1427.

Avital, S., I. Rog, S. Livne-Luzon, R. Cahanovitc, and T. Klein. 2022. Asymmetric belowground carbon transfer in a diverse tree community. Molecular ecology **31**:3481–3495.

Baldrian, P. 2017. Forest microbiome: diversity, complexity and dynamics. FEMS Microbiology reviews **41**:109–130.

Barnett, D. J., I. C. Arts, and J. Penders. 2021. microViz: an R package for microbiome data visualization and statistics. Journal of Open Source Software **6**:3201.

Callahan, B. J., P. J. McMurdie, M. J. Rosen, A. W. Han, A. J. A. Johnson, and S. P. Holmes. 2016. DADA2: High-resolution sample inference from Illumina amplicon data. Nature methods **13**:581–583.

Cotrufo, M. F., and J. M. Lavallee. 2022. Soil organic matter formation, persistence, and functioning: A synthesis of current understanding to inform its conservation and regeneration. Advances in agronomy **172**:1–66.

https://doi.org/10.5194/egusphere-2026-2099
Preprint. Discussion started: 23 April 2026

Cotrufo, M. F., M. G. Ranalli, M. L. Haddix, J. Six, and E. Lugato. 2019. Soil carbon storage informed by particulate and mineral-associated organic matter. Nature Geoscience **12**:989–994.

Crowther, T. W., J. Van den Hoogen, J. Wan, M. A. Mayes, A. Keiser, L. Mo, C. Averill, and D. S. Maynard. 2019. The global soil community and its influence on biogeochemistry. Science **365**:eaav0550.

Díaz-Martínez, P., F. T. Maestre, E. Moreno-Jiménez, M. Delgado-Baquerizo, D. J. Eldridge, H. Saiz, N. Gross, Y. Le Bagousse-Pinguet, B. Gozalo, and V. Ochoa. 2024. Vulnerability of mineral-associated soil organic carbon to climate across global drylands. Nature Climate Change **14**:976–982.

Díaz-Pinés, E., A. Rubio, H. Van Miegroet, F. Montes, and M. Benito. 2011. Does tree species composition control soil organic carbon pools in Mediterranean mountain forests? Forest Ecology And Management **262**:1895–1904.

Doetterl, S., A. Stevens, J. Six, R. Merckx, K. Van Oost, M. Casanova Pinto, A. Casanova-Katny, C. Muñoz, M. Boudin, and E. Zagal Venegas. 2015. Soil carbon storage controlled by interactions between geochemistry and climate. Nature Geoscience **8**:780–783.

Dror, D., and T. Klein. 2022. The effect of elevated CO2 on aboveground and belowground carbon allocation and eco-physiology of four species of angiosperm and gymnosperm forest trees. Tree Physiology **42**:831–847.

Fierer, N., and R. B. Jackson. 2006. The diversity and biogeography of soil bacterial communities. Proceedings of the National Academy of Sciences **103**:626–631.

Fuks, G., M. Elgart, A. Amir, A. Zeisel, P. J. Turnbaugh, Y. Soen, and N. Shental. 2018. Combining 16S rRNA gene variable regions enables high-resolution microbial community profiling. Microbiome **6**:17.

Georgiou, K., D. Angers, R. E. Champiny, M. F. Cotrufo, M. E. Craig, S. Doetterl, A. S. Grandy, J. M. Lavallee, Y. Lin, and E. Lugato. 2025. Soil carbon saturation: what do we really know? Global Change Biology **31**:e70197.

Georgiou, K., R. B. Jackson, O. Vindušková, R. Z. Abramoff, A. Ahlström, W. Feng, J. W. Harden, A. F. Pellegrini, H. W. Polley, and J. L. Soong. 2022. Global stocks and capacity of mineral-associated soil organic carbon. Nature communications **13**:3797.

Gill, R. A., and R. B. Jackson. 2000. Global patterns of root turnover for terrestrial ecosystems. The New Phytologist **147**:13–31.

Gregorich, E. G., H. Janzen, B. H. Ellert, B. L. Helgason, B. Qian, B. J. Zebarth, D. A. Angers, R. P. Beyaert, C. F. Drury, and S. D. Duguid. 2017. Litter decay controlled by temperature, not soil properties, affecting future soil carbon. Global Change Biology **23**:1725–1734.

Griscom, B. W., J. Adams, P. W. Ellis, R. A. Houghton, G. Lomax, D. A. Miteva, W. H. Schlesinger, D. Shoch, J. V. Siikamäki, and P. Smith. 2017. Natural climate solutions. Proceedings of the National Academy of Sciences **114**:11645–11650.

Hansen, P. M., R. Even, A. E. King, J. Lavallee, M. Schipanski, and M. F. Cotrufo. 2024. Distinct, direct and climate-mediated environmental controls on global particulate and mineral-associated organic carbon storage. Global Change Biology **30**:e17080.

Hayatsu, M., C. Katsuyama, and K. Tago. 2021. Overview of recent researches on nitrifying microorganisms in soil. Soil Science and Plant Nutrition **67**:619–632.

Hong, S., G. Yin, S. Piao, R. Dybzinski, N. Cong, X. Li, K. Wang, J. Peñuelas, H. Zeng, and A. Chen. 2020. Divergent responses of soil organic carbon to afforestation. Nature Sustainability **3**:694–700.

https://doi.org/10.5194/egusphere-2026-2099
Preprint. Discussion started: 23 April 2026

769 Itkin, D., A. Ronen, B. Needelman, O. Crouvi, and G. Eshel. 2025. Israel Soil Taxonomy GIS
770 (online version 2 — 1/2025).
771 Jakoby, G., I. Rog, S. Megidish, and T. Klein. 2020. Enhanced root exudation of mature
772 broadleaf and conifer trees in a Mediterranean forest during the dry season. Tree
773 Physiology **40**:1595–1605.
774 Jorgensen, T. D., S. Pornprasertmanit, A. M. Schoemann, and Y. Rosseel. 2012. semTools:
775 Useful tools for structural equation modeling. CRAN: Contributed Packages.
776 Knafo, M., S. Rezenman, T. Idan, M. Elgart, S. Dagan, Z. Reich, R. Kapon, D. Sade, and N.
777 Shental. 2023. CoSMIC-A hybrid approach for large-scale, high-resolution microbial
778 profiling of novel niches. bioRxiv:2023.2009. 2003.556087.
779 Lal, R., C. Monger, L. Nave, and P. Smith. 2021. The role of soil in regulation of climate.
780 Philosophical Transactions of the Royal Society B **376**:20210084.
781 Lavallee, J., R. Conant, E. Paul, and M. Cotrufo. 2018. Incorporation of shoot versus root-
782 derived 13C and 15N into mineral-associated organic matter fractions: results of a soil
783 slurry incubation with dual-labelled plant material. Biogeochemistry **137**:379–393.
784 Lin, H., and S. D. Peddada. 2020. Analysis of compositions of microbiomes with bias
785 correction. Nature communications **11**:3514.
786 Lindahl, B. D., and A. Tunlid. 2015. Ectomycorrhizal fungi–potential organic matter
787 decomposers, yet not saprotrophs. New Phytologist **205**:1443–1447.
788 Ll, H., X. Li, Z. Dou, J. Zhang, and C. Wang. 2012. Earthworm (Aporrectodeatrapezoides)–
789 mycorrhiza (Glomus intraradices) interaction and nitrogen and phosphorus uptake by
790 maize. Biology and Fertility of Soils **48**:75–85.
791 Lucas-Borja, M. E., D. Candel, K. Jindo, J. Moreno, M. Andrés, and F. Bastida. 2012. Soil
792 microbial community structure and activity in monospecific and mixed forest stands,
793 under Mediterranean humid conditions. Plant and Soil **354**:359–370.
794 Ma, Y., J. Wang, Y. Liu, X. Wang, B. Zhang, W. Zhang, T. Chen, G. Liu, L. Xue, and X.
795 Cui. 2023. Nocardioides:“specialists” for hard-to-degrade pollutants in the
796 environment. Molecules **28**:7433.
797 McMurdie, P. J., and S. Holmes. 2013. phyloseq: an R package for reproducible interactive
798 analysis and graphics of microbiome census data. PloS one **8**:e61217.
799 Nissan, A., U. Alcolombri, N. Peleg, N. Galili, J. Jimenez-Martinez, P. Molnar, and M.
800 Holzner. 2023. Global warming accelerates soil heterotrophic respiration. Nature
801 communications **14**:3452.
802 Obersteiner, S., and T. Klein. 2022. Closing in on the last frontier: C allocation in the
803 rhizosphere. Global Change Biology **28**:6835.
804 Obersteiner, S. O.-S., Yaara; Yalin, David; Sade, Dagan; Zavaro, Vered; Reich, Ziv; Klein,
805 Tamir 2026. Pine root exudate terpenoids associate with Mycobacterium sp. under
806 summer drought in a mixed Mediterranean forest. Environmental Microbiome.
807 **submitted, under review**.
808 Olsen, S. R. 1954. Estimation of available phosphorus in soils by extraction with sodium
809 bicarbonate. US Department of Agriculture.
810 Oppenheimer-Shaanan, Y., G. Jakoby, M. L. Starr, R. Karliner, G. Eilon, M. Itkin, S.
811 Malitsky, and T. Klein. 2022. A dynamic rhizosphere interplay between tree roots and
812 soil bacteria under drought stress. Elife **11**:e79679.
813 Peoples, M. B., K. E. Giller, E. S. Jensen, and D. F. Herridge. 2021. Quantifying country-to-
814 global scale nitrogen fixation for grain legumes: I. Reliance on nitrogen fixation of
815 soybean, groundnut and pulses. Plant and Soil **469**:1–14.
816 Poeplau, C., A. Don, J. Six, M. Kaiser, D. Benbi, C. Chenu, M. F. Cotrufo, D. Derrien, P.
817 Gioacchini, and S. Grand. 2018. Isolating organic carbon fractions with varying

https://doi.org/10.5194/egusphere-2026-2099
Preprint. Discussion started: 23 April 2026

turnover rates in temperate agricultural soils–A comprehensive method comparison. Soil Biology and Biochemistry **125**:10–26.

Rasmussen, C., K. Heckman, W. R. Wieder, M. Keiluweit, C. R. Lawrence, A. A. Berhe, J. C. Blankinship, S. E. Crow, J. L. Druhan, and C. E. Hicks Pries. 2018. Beyond clay: towards an improved set of variables for predicting soil organic matter content. Biogeochemistry **137**:297–306.

Rezenman, S., M. Knafo, I. Tsigalnitski, S. Barad, G. Jona, D. Levi, O. Dym, Z. Reich, and R. Kapon. 2023. gUMI-BEAR, a modular, unsupervised population barcoding method to track variants and evolution at high resolution. PloS one **18**:e0286696.

Rog, I., B. Hilman, H. Fox, D. Yalin, R. Qubaja, and T. Klein. 2024. Increased belowground tree carbon allocation in a mature mixed forest in a dry versus a wet year. Global Change Biology **30**:e17172.

Rog, I., G. Jakoby, and T. Klein. 2021a. Carbon allocation dynamics in conifers and broadleaved tree species revealed by pulse labeling and mass balance. Forest Ecology And Management **493**:119258.

Rog, I., O. Lewin-Epstein, S. Livne-Luzon, L. Hadany, and T. Klein. 2022. Prosperity of the commons: Generalist mycorrhizal species dominate a mixed forest and may promote forest diversity by mediating resource sharing among trees. bioRxiv:2022.2008. 2001.502298.

Rog, I., C. Tague, G. Jakoby, S. Megidish, A. Yaakobi, Y. Wagner, and T. Klein. 2021b. Interspecific soil water partitioning as a driver of increased productivity in a diverse mixed Mediterranean forest. Journal of geophysical research: Biogeosciences **126**:e2021JG006382.

Rosseel, Y. 2012. lavaan: An R package for structural equation modeling. Journal of Statistical Software **48**:1–36.

Rowley, M. C., S. Grand, and É. P. Verrecchia. 2018. Calcium-mediated stabilisation of soil organic carbon. Biogeochemistry **137**:27–49.

Schmidt, M. W., M. S. Torn, S. Abiven, T. Dittmar, G. Guggenberger, I. A. Janssens, M. Kleber, I. Kögel-Knabner, J. Lehmann, and D. A. Manning. 2011. Persistence of soil organic matter as an ecosystem property. Nature **478**:49–56.

Six, J., S. Doetterl, M. Laub, C. R. Müller, and M. Van de Broek. 2024. The six rights of how and when to test for soil C saturation. Soil **10**:275–279.

Sokol, N. W., E. D. Whalen, A. Jilling, C. Kallenbach, J. Pett-Ridge, and K. Georgiou. 2022. Global distribution, formation and fate of mineral-associated soil organic matter under a changing climate: A trait-based perspective. Functional Ecology **36**:1411–1429.

Spohn, M., S. Bagchi, L. A. Biederman, E. T. Borer, K. A. Bråthen, M. N. Bugalho, M. C. Caldeira, J. A. Catford, S. L. Collins, and N. Eisenhauer. 2023. The positive effect of plant diversity on soil carbon depends on climate. Nature communications **14**:6624.

Stell, E., D. Warner, J. Jian, B. Bond-Lamberty, and R. Vargas. 2021. Spatial biases of information influence global estimates of soil respiration: How can we improve global predictions? Global Change Biology **27**:3923–3938.

Urbanová, M., J. Šnajdr, and P. Baldrian. 2015. Composition of fungal and bacterial communities in forest litter and soil is largely determined by dominant trees. Soil Biology and Biochemistry **84**:53–64.

Whalen, E. D., A. S. Grandy, N. W. Sokol, M. Keiluweit, J. Ernakovich, R. G. Smith, and S. D. Frey. 2022. Clarifying the evidence for microbial-and plant-derived soil organic matter, and the path toward a more quantitative understanding. Global Change Biology **28**:7167–7185.

https://doi.org/10.5194/egusphere-2026-2099
Preprint. Discussion started: 23 April 2026

866 Wolińska, A., A. Kuźniar, U. Zielenkiewicz, A. Banach, D. Izak, Z. Stępniewska, and M.
867 Błaszczyk. 2017. Metagenomic analysis of some potential nitrogen-fixing bacteria in
868 arable soils at different formation processes. Microbial Ecology **73**:162–176.
869 Wu, J., H. Zhang, Y. Pan, X. Cheng, K. Zhang, and G. Liu. 2023. Particulate organic carbon
870 is more sensitive to nitrogen addition than mineral-associated organic carbon: A meta-
871 analysis. Soil and Tillage Research **232**:105770.
872 Yuste, J. C., A. Fernandez-Gonzalez, M. Fernandez-Lopez, R. Ogaya, J. Penuelas, J. Sardans,
873 and F. Lloret. 2014. Strong functional stability of soil microbial communities under
874 semiarid Mediterranean conditions and subjected to long-term shifts in baseline
875 precipitation. Soil Biology and Biochemistry **69**:223–233.
876 Yuste, J. C., J. Peñuelas, M. Estiarte, J. GARCIA-MAS, S. Mattana, R. Ogaya, M. Pujol, and
877 J. Sardans. 2011. Drought-resistant fungi control soil organic matter decomposition
878 and its response to temperature. Global Change Biology **17**:1475–1486.

879

https://doi.org/10.5194/egusphere-2026-2099
Preprint. Discussion started: 23 April 2026

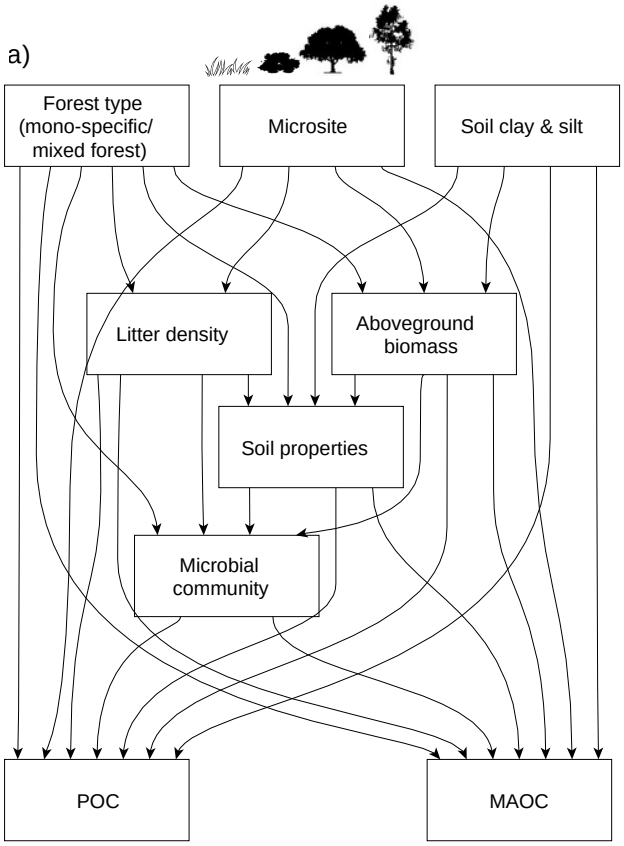

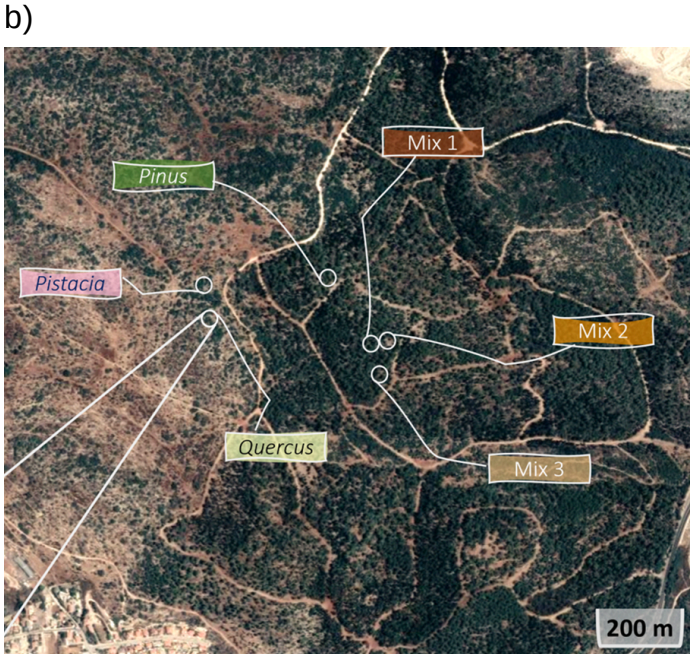

Figure 1: (a) a path diagram. We hypothesized that forest characteristics (mono-specific/mixed forest) and microsite (*Pistacia*, *Pinus, Quercus* or forest gap, affect MAOC and POC concentrations either directly or indirectly by affecting tree species traits (biomass and litter density), soil properties and the microbial community. Also, we hypothesized that the soil C capacitance will be constrained by the soil clay & silt ,content. (b) an aerial map displaying six plots within Yishi Forest (mono-specific plots dominated by *Pistacia* ".*Pinus* or *Quercus* trees (n=39) and three mixed forest plots(n=27)). Satellite imagery © Google Earth

https://doi.org/10.5194/egusphere-2026-2099
Preprint. Discussion started: 23 April 2026

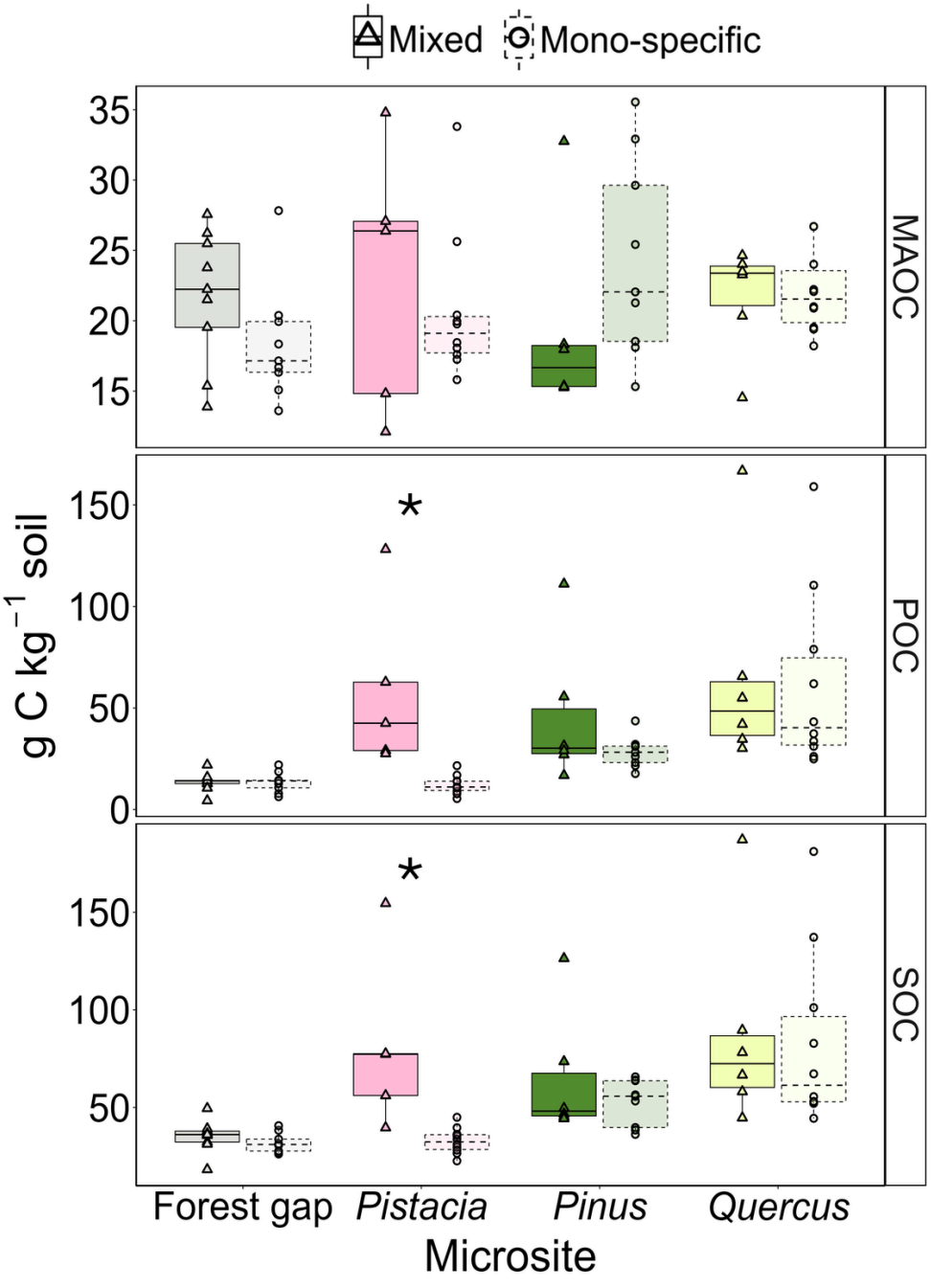

Figure. 2. SOC concentrations partitioned across different forest types and microsites within the forest in Yishi (from top to bottom: mineral-associated (MAOC), particulate (POC) and total soil organic carbon (SOC)). Box Plots are categorized by the microsite under the dominant tree canopy i.e., Pistacia, Pinus, Quercus, or open forest gaps (n = 66). Box plots are further categorized into) two groups based on forest composition: mono-specific forest (faded color, dashed, plus shape, n and mixed forest (fully saturated color, plain, round shape, n = 27). Box plots display the (39 = .median, first and third quartiles, and whiskers extending to 1.5 times the interquartile range Asterisks indicate significant contrasts ($p < 0.05$) between mixed and mono-specific forest plots .within microsites. ***$p < 0.001$; **$p < 0.01$; *$p < 0.05$

https://doi.org/10.5194/egusphere-2026-2099
Preprint. Discussion started: 23 April 2026

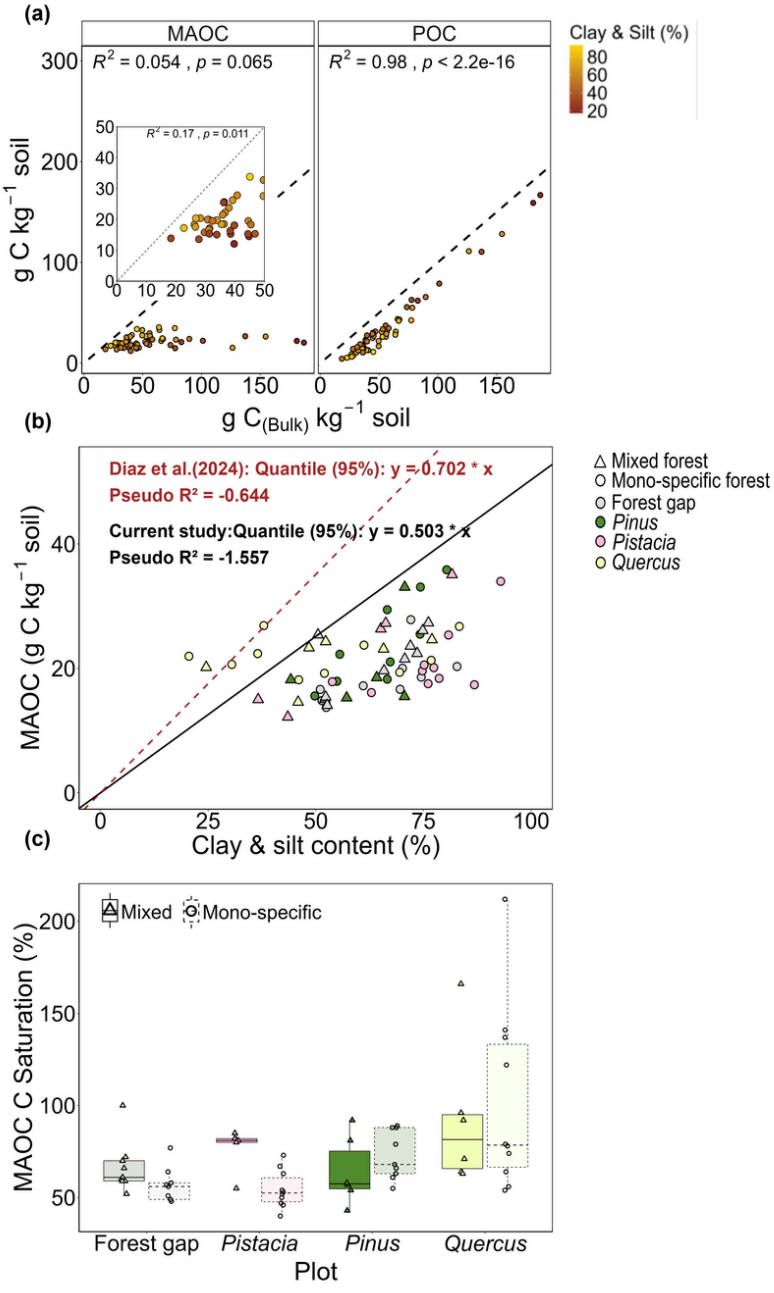

Figure. 3. Mineral-associated and particulate organic carbon in our observational synthesis. (a) Mineral-associated organic carbon (MAOC) and particulate organic carbon (POC) as functions of total ,soil organic carbon (SOC). The color gradient represents varying percentages of clay and silt content and the dashed lines represent 1:1 relationships. (b) Mineral-associated organic carbon (MAOC; g C kg^{-1} soil) as a function of clay and silt content (%). The maximum slope (fit as the 95th quantile) .represents the intrinsic capacity of minerals to store carbon, which depends on mineral composition The dashed line represents a similar calculation based on data from Díaz-Martínez et al., (2024) (c) Percent mineralogical C saturation—the proximity of a soil to its mineralogical carbon capacity was calculated for each measurement. % C saturation is grouped by the soil sample—(MAOCmax) location under the dominant tree canopy (i.e., Pistacia, Pinus or Quercus, n = 48) or open forest gaps and by forest composition: mono-specific forest (faded color, dashed, plus shape, n = 39) and (n = 18) .mixed forest (fully saturated color, plain, round shape,n = 27)

https://doi.org/10.5194/egusphere-2026-2099
Preprint. Discussion started: 23 April 2026

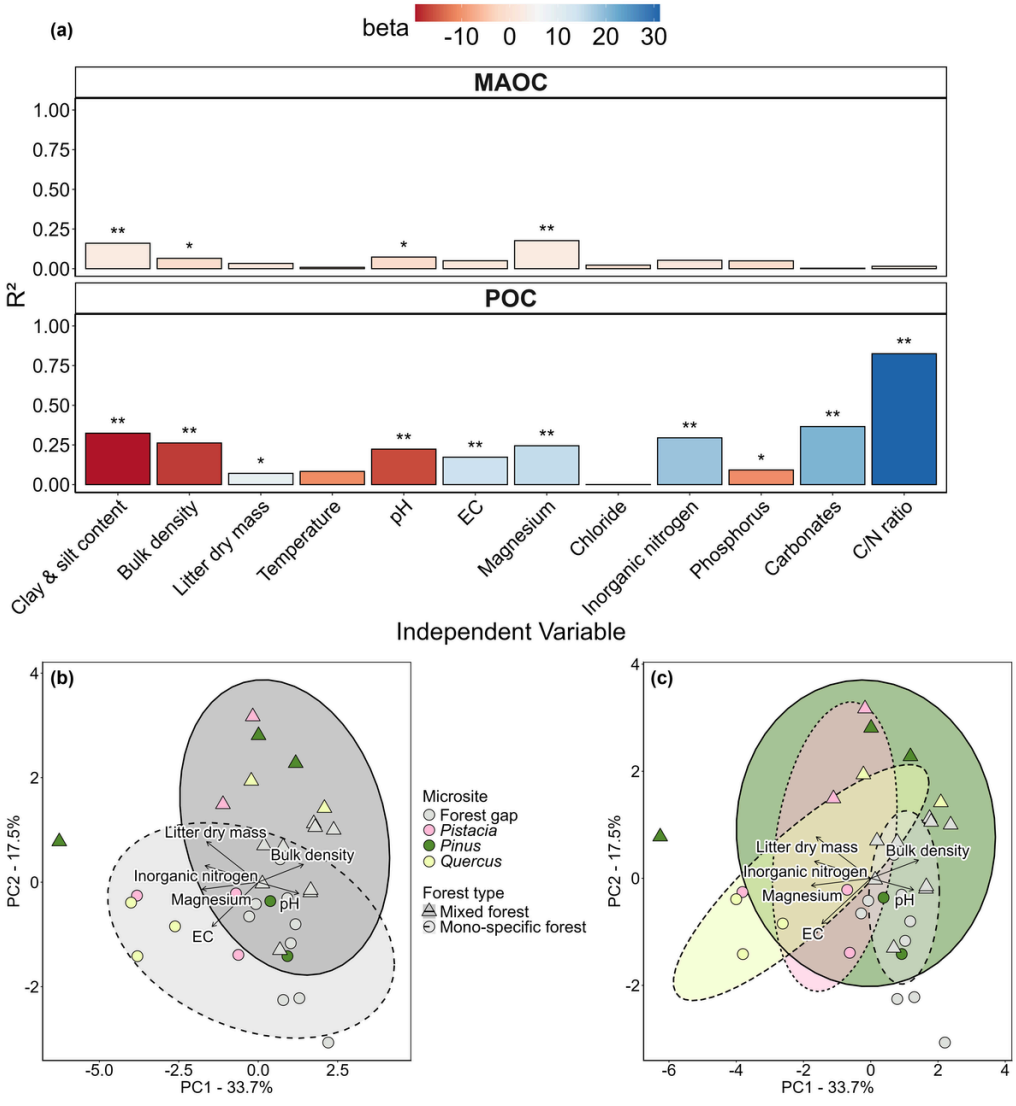

Fig. 4. Models of the effects of soil physical and chemical properties. (a) Individual mixed regression models assessed the relationship between each predictor variable and the response variable. Estimated coefficients of the explanatory variables (β) are represented by a color gradient, with significance levels indicated (*p < 0.05, **p < 0.01). (b,c) Principal .component analysis (PCA) biplot showing soil physicochemical properties Points represent individual samples colored by microsite and shaped by forest type. Ellipses indicate the 95% confidence intervals for either forest type (b) or (c) microsite. Vectors represent the loadings of selected soil variables (loading magnitude > 0.4) on the first two principal components with arrow length indicating the strength and direction of ,(PC1 and PC2) .contribution

https://doi.org/10.5194/egusphere-2026-2099
Preprint. Discussion started: 23 April 2026

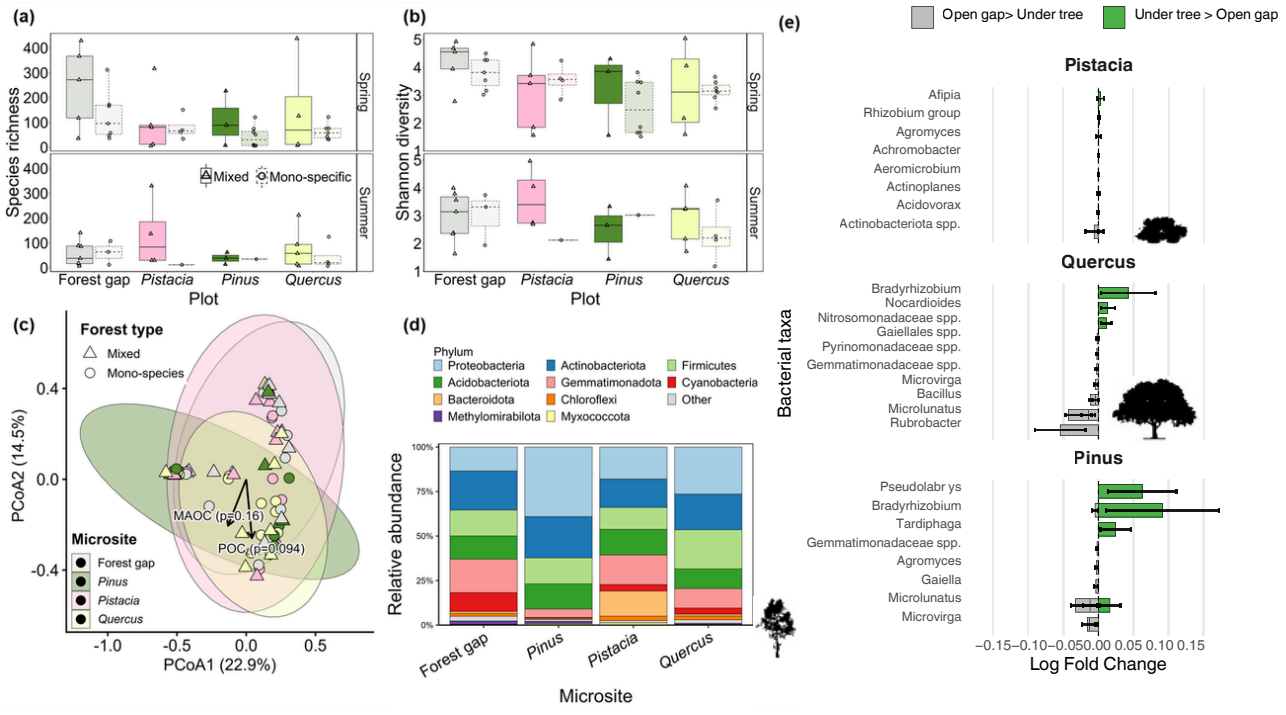

Fig. 5. Bacterial community structure and diversity across microsites and forest types in Yishi. (a) Species ,richness and (b) Shannon diversity index of bacterial communities, categorized by microsite (forest gap Pistacia, Pinus, and Quercus) and season (spring, summer). Box plots are further divided by forest composition: mono-specific forests (faded color, dashed box, plus symbol, n = 39) and mixed forests (fully saturated color, solid box, circle symbol, n = 27). (c) Principal Coordinates Analysis (PCoA) plot based on :beta diversity, showing clustering by microsite and forest type. Points represent individual samples (circles mixed forests; triangles: mono-specific forests), colored by microsite. Ellipses represent 95% confidence ,intervals around group centroids. The axes indicate the percentage of variation explained (PCoA1: 22.9% PCoA2: 14.5%). (d) Relative composition of the top 10 bacterial genera, displayed as 100% stacked horizontal bars per genus, showing the proportion contributed by each microsite. Genus names are listed on .the right. Samples were collected from six plots in Yishi Forest during spring (n = 43) and summer (n = 28) .Microsites include dominant tree canopies (Pistacia, Pinus, Quercus; n = 48) or open forest gaps (n = 18) .Box plots display the median, interquartile range (IQR), and whiskers extending to 1.5 × IQR

https://doi.org/10.5194/egusphere-2026-2099
Preprint. Discussion started: 23 April 2026

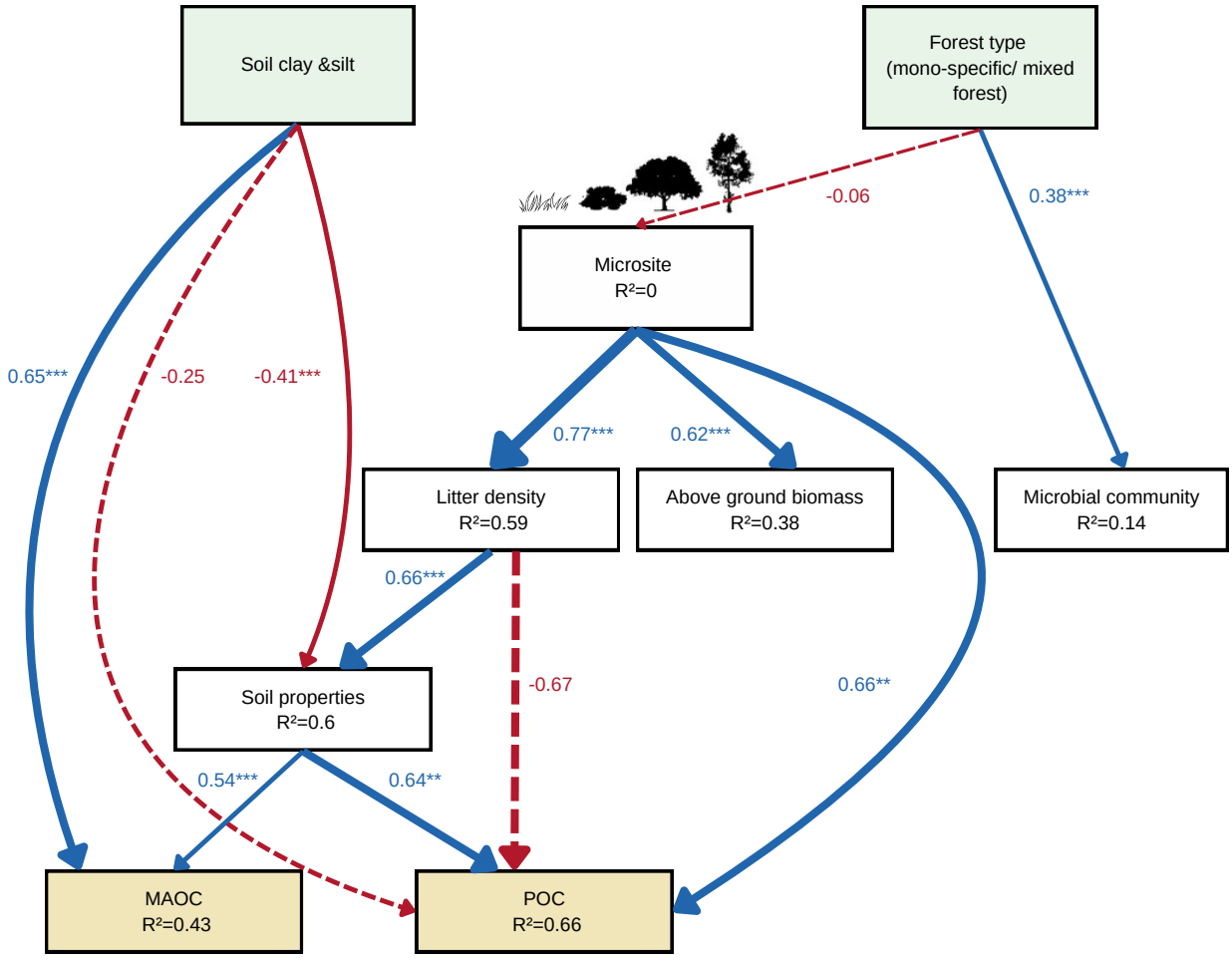

Fig. 6. A graphical representation showing all the statistically-significant paths retained in the final model. Boxes represent measured variables and paths are represented by arrows. The width of the arrow is scaled based on the magnitude of the standardized regression coefficient, with blue arrows indicating a positive correlation and red arrows a negative correlation. Significant paths ($p \leq 0.05$) or marginally significant paths ($p \leq 0.1$) are indicated by a solid/ dashed line, respectively. A full list of the coefficient values, including non-significant paths that were retained in the final model, is presented in .Supplementary Table S1